Submitted to JCTC, 12/18/2023, revised 1/25/2024

A New Full-dimensional Reactive Potential Energy Surface for the H_4 System

Yang Liu,[1] Pablo G. Jambrina,[2] James F. E. Croft,[3] Naduvalath. Balakrishnan,[4] F. Javier Aoiz,[5] and Hua Guo[1,*]

[1]*Department of Chemistry and Chemical Biology, Center for Computational Chemistry, University of New Mexico, Albuquerque, New Mexico 87131, USA*

[2]*Departamento de Quimica Fisica, Universidad de Salamanca, Salamanca 37008, Spain*

[3]*The Dodd-Walls Centre for Photonic and Quantum Technologies, New Zealand and Department of Physics, University of Otago, Dunedin 9054, New Zealand*

[4]*Department of Chemistry and Biochemistry, University of Nevada, Las Vegas, Nevada 89154, USA*

[5]*Departamento de Quimica Fisica, Universidad Complutense, Madrid 28040, Spain*

*: Corresponding author, email: hguo@unm.edu (HG)

Abstract

As the most abundant molecule in the universe, collisions involving H_2 have important implications in astrochemistry. Collisions between hydrogen molecules also represent a prototype for assessing various dynamic methods for understanding fundamental few-body processes. In this work, we develop a new and highly accurate full-dimensional potential energy surface (PES) covering all reactive channels of the $H_2 + H_2$ system, which extends our previously reported $H_2 + H_2$ nonreactive PES [J. Chem. Theory Comput. 2021, 17, 6747] by adding 39,538 additional ab initio points calculated at the MRCI/AV5Z level in the reactive channels. The global PES is represented with high-fidelity (RMSE = 0.6 meV for a total of 79,000 points) by a permutation invariant polynomial-neural network (PIP-NN), and is suitable for studying collision induced dissociation, single exchange, as well as four center exchange reactions. Preliminary quasi-classical trajectory studies on the new PIP-NN PES reveal strong vibrational enhancement of all reaction channels.

I. Introduction

The hydrogen molecule (H_2) and its isotopomers are the most abundant molecular species in the universe and play a vital role in many areas of astrophysics and astrochemistry.[1] In interstellar media, the evolution of shock fronts and photodissociation regions is governed by the energy transfer involving H_2 molecules.[2, 3] Collision induced energy transfer between H_2 molecules and between H_2 and other species is also the main contributor to the cooling of the primordial gas[4, 5] and heat generation through shock waves.[6] In interstellar molecular clouds, molecular hydrogen, the primary component of these clouds, can undergo internal excitation and collision induced dissociation due to the elevated temperatures resulting from shock wave compressions.[2] Unfortunately, H_2 and D_2 are not easily detected due to lack of electric dipole moment, but spectroscopic signatures of HD have been detected in space.[7]

Molecular hydrogen is also involved in various extreme environments (e.g., high vibrational excitations and collision energies) such as combustion[8] and plasmas,[9] where the collisional energy transfer between ro-vibrationally excited H_2 molecules is an important part of the chemistry.[10, 11]

Due to experimental difficulties in simulating extreme conditions, energy transfer processes between two H_2 molecules (and their isotopic variants) have largely been investigated theoretically.[12-33] These calculations were carried out either in full-dimensionality or within the rigid rotor approximation using various potential energy surfaces (PESs).[8, 34-42] More recently, this system has been leveraged in experimental studies of cold collisions involving aligned H_2/HD/D_2 molecules,[43-47] using the Stark-induced Adiabatic Raman Passage (SARP) technique.[48] Quantum mechanical calculations by some of the authors of this paper helped to elucidate the role of shape resonances in the stereodynamics of these prototypical systems.[49-52]

When considering scattering between H_2 molecules at sufficiently high collision energies, various reactive processes may occur, in addition to elastic and inelastic scattering. Firstly, there is collision induced dissociation (CID), in which one of the H-H bonds is cleaved:

$$HH + H'H' \rightarrow HH + H' + H'. \quad (R1)$$

Secondly, the H-H bond cleavage in both molecules might be associated with the formation of a new H_2 molecule, in what is called single exchange (SE) reaction, which implies the breaking of two bonds and the formation of new one:

$$HH + H'H' \rightarrow H + HH' + H'. \quad (R2)$$

Finally, the reaction can take place in the so-called four center (4C) exchange, in which both reactant molecules break their bonds leading to two new hydrogen molecules,

$$HH + H'H' \rightarrow HH' + HH'. \quad (R3)$$

Different from a more prevalent three-center reaction, where only one bond is broken while another is formed during the course of reaction, a 4C reaction entails a simultaneous cleavage and formation of two bonds.[53] In organic chemistry, 1,3-dipolar cycloaddition and Diels-Alder reactions all proceed with a 4C transition state. As the simplest 4C reaction, R3 has been extensively investigated in the past.[54-65] The Woodward-Hoffmann rules dictate that a 4C barrier is necessarily high as it involves two electron excitation.[66] To provide a comprehensive understanding of the reaction dynamics, it is essential to have an accurate global PES. Unfortunately, most existing H_4 PESs,[8, 34, 36, 37, 39-41] including the latest one constructed by us,[42] are designed for non-reactive scattering, thus not suitable for reactive studies.

By fitting 48,180 energy points at the level of multi-reference (single and) double excitation configuration interaction (MRD-CI) with the (9s3p1d)/[4s3p1d] Gaussian basis set, Boothroyd, Martin, Keogh, and Peterson (BMKP) constructed a full-dimensional reactive PES for the H_4 system

more than 20 years ago.[38] While this PES covers all reactive channels, quantum non-reactive scattering calculations have found it to be inaccurate in the long range.[18-21, 23-25, 67] In a recent publication, Zuo, Croft, Balakrishnan, and Guo (ZCBG) reported a new non-reactive full-dimensional PES for the H_2 + H_2 system.[42] A total of 39,462 ab initio points at the level of multi-reference configuration interaction (MRCI)[68, 69] with the augmented correlation-consistent polarized valence 5-zeta (AV5Z) basis set[70, 71] was fitted using the permutation invariant polynomial-neural network (PIP-NN) fitting method,[72, 73] with a root mean square error (RMSE) of only 0.44 cm^{-1}. This ZCBG PES demonstrates the correct long-range behavior for the H_2 + H_2 asymptote and covers a large range of H-H distances, enabling vibrational excitation of the molecules. Quantum non-reactive scattering calculations[42] have found good agreement with those obtained on the accurate Hinde PES[39] based on CCSD(T) data.

In this work, we extend the ZCBR PES to include all reactive channels, *i.e.*, the CID, SE, and 4C reactions. The new global reactive PES is fitted to a total of 79,000 ab initio points at the MRCI/AV5Z level using the PIP-NN method. Preliminary quasi-classical trajectory (QCT) calculations are carried out using this PES to investigate the reactive scattering, with an aim to understand possible vibrational enhancement of the reactive events. The remaining part of this publication is organized as follows: in Section II, the ab initio and PIP-NN fitting methods are presented. Section III reports the features of the new PES and QCT results on the PES. Section IV is the conclusions.

II. Methods

II.A. Ab Initio Calculations

The 2015.1.0 version of the MOLPRO program package[74] was employed to perform all electronic structure calculations. The energies, frequencies, and geometries of all the stationary points,

as shown **Figure 1** and **Table 1**, were determined at the MRCI/AV5Z level. To this end, the spin-restricted Hartree-Fock (RHF) wave functions were first employed as the basis for subsequent complete active space self-consistent field (CASSCF) calculations, in which all four electrons in four orbitals (4e and 4o) were included. The calculated wave functions were then used as the reference for the subsequent MRCI calculations. In this work, The Davidson correction[75] was chosen to promote size extensivity and account for higher-order excitations.

II.B. Construction of the Potential Energy Surface

To extend the previous ZCBG PES to the reactive channels, QCT calculations with a high vibrational excitation of H_2 ($v = 14$) and the collision energy of 2.0 eV were performed on the previous PES to explore all the relevant reactive channels *i.e.*, the CID, SE, and 4C reactions. The new points generated from the QCT calculations were added to the dataset to improve the PES in the corresponding configuration space. This procedure was repeated until (a) no spurious features were found, (b) the reaction probability of the three reactive channels was converged, and (c) the key properties of the system, including the geometries, energies, frequencies of all stationary points, as well as the reaction paths were well reproduced.

The new reactive PES was fit to the enlarged ab initio dataset using the PIP-NN method[72, 73] with the following functional form,

$$V = b_1^{(3)} + \sum_{k=1}^{K} \left(\omega_{1,k}^{(3)} \cdot f_2 \left(b_k^{(2)} + \sum_{j=1}^{J} \left(\omega_{k,j}^{(2)} \cdot f_1 \left(b_j^{(1)} + \sum_{i=1}^{I} \omega_{j,i}^{(1)} \cdot G_i \right) \right) \right) \right) \quad (1)$$

where I denotes the size of the PIP input layer with $G_i = \hat{S} \prod_{i<j}^{N} p_{ij}^{l_{ij}}$. $p_{ij} = \exp(-\lambda r_{ij})$ represents the Morse-like variables associated with internuclear distances (r_{ij}),[76] these variables are linked to an adjustable constant denoted as λ (chosen to be 2.0 bohr in this work). $\hat{S}$ denotes the symmetrization operator used to keep the permutation invariance of identical atoms in the system; $\omega_{j,i}^{(l)}$ and $b_j^{(l)}$

represent the weight connecting the ith neuron of the (l-1)th layer to the jth neuron of the lth layer and the bias of the jth neuron in the lth layer, respectively. J and K are the numbers of neurons in the hidden layers. For the H_4 system, 39 PIPs up to the fifth order were used as the input of the NN fitting. The PIPs was obtained by the Monomial Symmetrization Approach (MSA) package.[77]

The parameters ω and b were optimized by minimizing the root mean square error (RMSE),

$$\mathrm{RMSE}=\sqrt{\sum_{i=1}^{N_{\mathrm{data}}}\left(E_{\mathrm{output}}^{i}-E_{\mathrm{target}}^{i}\right)^{2}/N_{\mathrm{data}}}. \quad (2)$$

To mitigate the problem of "overfitting" we implemented the "early stopping" method[78] in which the dataset was randomly divided into three segments: training (90%), validation (5%), and test (5%). The minimization process is stopped when the performance on the validation set shows no further improvement for a defined number of consecutive epochs. To minimize random errors of the nonlinear fitting, the final NN PES was chosen as the average of three best fittings. It should be noted that the long-range interaction terms used in the ZCBG PES[42] can be readily interfaced with the new reactive PES to provide accurate description for low energy collision processes.

II.C. Quasi-Classical Trajectory Calculations

QCT calculations were performed on the new PIP-NN PES using the VENUS program.[79] The initial vibrational states were set to v_1 = 10, 11, 12, and 13 for one of two H_2 molecules and v_2 = 0 for the other. The Einstein-Brillouin-Keller (EBK) semiclassical quantization approach[80] was used to calculate the corresponding vibrational energies. Both collision partners were initially rotationless. The initial translational energy between the two molecules was increased from 0.1 to 1.6 eV with the step of 0.1 eV. To ensure good energy and angular momentum conservation, the integration time step was set to 0.05 fs. The gradient was computed numerically. The trajectories were initiated with the two reactants separated by 8 Å, at which the interaction potential is insignificant compared to the

collision energy. For the nonreactive and 4C channels, the integration was terminated when the two hydrogen molecules were separated by 8 Å. Following the strategy used in Ref. [60], the trajectories were stopped when at least four diatomic distances are larger than 8.0 Å for the dissociation channels, *i.e.*, the CID and SE processes. A total of 50,000 trajectories were sampled for each set of initial conditions, which yielded statistical errors less than 5.0%. The impact parameter b was sampled between 0 and the maximum impact parameter b_{max} according to $b = b_{max}(\mathrm{RND})^{1/2}$, where RND is a random number between 0 and 1. The parameter b_{max} was determined using small batches of trajectories with trial values. The determined b_{max} ranges from 1.4 to 3.3 Å under various initial conditions.

The classical treatment of the dynamics might not preserve the zero-point energy (ZPE) in the H_2 product, and this ZPE violation is particularly severe for endoergic processes such as SE and 4C reactions. To address this issue, we have included only those trajectories with vibrational energies exceeding its ZPE after collision.

Finally, the reactive integral cross sections (ICSs) for CID, SE, and 4C processes are all computed according to the following formula:

$$\sigma_r\left(E_c\right) = \pi b_{\max}^2(E_c) P_r\left(E_c\right), \tag{3}$$

where $P_r(E_c)$ is the reaction probability at the specified collision energy E_c. The reaction probabilities are given by the ratios N_{CID}/N_{total}, N_{SE}/N_{total}, and N_{4C}/N_{total} for the CID, SE, and 4C channels, respectively. N_{CID}, N_{SE}, and N_{4C} denote the numbers of trajectories found in the CID, SE, 4C channels, respectively, while N_{total} is the total number of trajectories. For comparison, we also performed the same QCT calculations on the BKMP PES.

III. Results

III.A. Ab Initio Calculations

Figure 1 illustrates the reaction pathways for the SE and 4C channels, as well as the optimized geometries of the transition states at the MRCI/AV5Z level. The corresponding energies and harmonic frequencies are listed in **Table 1**, along with the values from the BKMP PES. In the SE channel, the transition state (TS1) has a linear geometry with an energy of 4.827 eV at the MRCI/AV5Z level, which is 0.295 eV larger than the transition state TS2 of the 4C reaction, which has a rhomboid structure. This structure is very different from a conventional 3C transition state because it features concurrent dual bond-breaking and bond-forming. Compared to the BMKP PES, the maximum deviations in the energy, frequencies, and bond lengths of TS2 are 0.033 eV, 387 cm^{-1}, and 0.02 Å, respectively. These differences are most likely attributable to the lower level of theory, smaller number of points, and less flexible functional form used in the construction of the BMKP PES.[38]

III.B. Potential Energy Surface

In addition to the original ab initio points generated in constructing the ZCBG PES,[42] additional 39538 new points were sampled to cover the three reactive channels. The new reactive PES is obtained by fitting a total of 79,000 points using the PIP-NN method. This number is significantly larger than that used in the BMKP fit (48,180).[38] After some tests, an NN structure was selected with 30 and 20 neurons in the two hidden layers, respectively, yielding 1841 nonlinear fitting parameters with the final average RMSE of 0.6 meV, which is much less than that of BMKP PES, 38.9 meV. This improved fitting quality can be attributed to the high fidelity of the PIP-NN method.[81] The fitting error as a function of the ab initio energies are shown in **Figure 2a** and the corresponding distribution of the fitting errors is depicted in **Figure 2b**. As can be seen, most of the points have very small fitting errors, and are evenly distributed along the energy up to 26 eV and about 81% of the data points have

fitting errors under 0.2 meV. The few outliers near 5 eV are mostly in the H_2 + 2H asymptote.

Figure 3a and **3b** show the potential energies along the minimum energy paths (MEPs) of TS1 and TS2, respectively, on the PIP-NN PES. The ab initio values along the MEPs are calculated and shown in the same figure for comparison. The agreement between the PES and direct ab initio calculations is excellent. The two-dimensional contour plot of the PES for the SE channel along R_1 and R_2 (defined in the same figure) with other coordinates fixed at TS1 is shown in **Figure 4**. As shown, the PES is smooth along the reaction path from the reactant asymptote to TS1 and the product asymptote. Clearly, TS1 is a "late" barrier, which suggests that vibrational excitation of the reactants should be able to enhance reactivity. **Figure 5** presents the contour plot of the PES for the 4C channel along R_1 and R_2 with other coordinates constrained at TS2. It can be seen that the 4C reaction channel is symmetric. Namely, the reactant side and the product side are equivalent to each other, and the corresponding transition state (TS2) features concurrent bond formation and bond breaking. It is also easy to see that the H-H bonds of the reactants are stretched extensively, suggesting that the 4C reaction has also a "late" barrier. Hence, vibrational excitation in the reactants might be more efficient than the collision energy in promoting the reaction.

III.C. Quasi-Classical Trajectory Calculations

The QCT calculated ICSs of the CID, 4C, and SE channels for the collision between H_2 (v_1 = 10, 11, 12, 13, j_1 = 0) and H_2 (v_2 = 0, j_2 = 0) on the PIP-NN PES (solid line) and BKMP PES (dotted line) are compared in **Figure 6** as a function of the collision energy (left-hand panels) and total energy (right-hand panels). Though he newly fitted PIP-NN PES is based on higher level of ab initio calculations and has lower fitting errors, the calculated ICSs are close to those on the BMKP PES as shown in **Figure 6**. In our opinion, this is due to the high barriers of the reactive channels. The barrier height of SE and CID channels are 4.827 and 4.532 eV, but the energy deviations between the two

PESs are only 0.003 and 0.027 eV for TS1 and TS2, respectively. As these processes are controlled largely by the barriers, the BMKP PES yields similar results.

Figure 6 clearly shows a positive correlation between the collision energy and ICSs is observed for all reactive channels. This is consistent with the activated nature of this reaction. As shown in the right-hand panels of **Figure 6**, vibrational excitation is more effective than the translational energy in promoting all three reactions because the ICS is larger when a hydrogen molecule has higher vibrational excitation at the same total energy. This vibrational enhancement can be traced back to the "late" barriers of the three reactions. For R1, the CID transition state is in the H_2 + H + H asymptote, which is a "late" barrier. According to Polanyi rules,[82] a later barrier is easier to be overcome by reactant vibration. For R2, the SE transition state (TS1) is already shown in **Figure 4** to be quite "late". Similarly, the 4C transition state (TS2) also features extended H-H distances, implying possible enhancement of the reactivity by reactant vibrational excitation.

We have recently proposed the Sudden Vector Projection (SVP) model[83] as a generalization of the Polanyi rules. The basic premise of SVP is that the reactant mode with the largest projection onto the reaction coordinate at the transition state has the best chance in promoting the reaction. The SVP values for TS1 and TS2 are presented in **Table 2**. According to these SVP predictions, both the reactant vibrational and translational modes are strongly coupled with the reaction coordinates, suggesting that excitations in these modes are expected to enhance the reactivity. On the other hand, the rotational modes have essentially no effect. These predictions are borne out qualitatively by the ICSs in **Figure 6**. The slightly larger SVP values for the transitional mode suggests that its excitation should be more effective than the same amount of vibrational excitation in promoting reaction, which is opposite to the results in **Figure 6**. This discrepancy might be due to the fact that the current calculations have focused on a highly excited H_2 reactant, while SVP is more appropriate in predicting

lower reactant vibrational excitations.

The CID reaction (R1) is the dominant process over the energy range considered, as the calculated ICSs are about ten times the corresponding values of the SE (R2) and 4C (R3) processes. The threshold of the CID reaction is strongly dependent on the vibrational excitation of a hydrogen molecule, much more so than the 4C and SE processes. For low vibrationally excited hydrogen reactants, additional energy is needed to reach its dissociation limit, and this can only be supplied by the collision energy. But this need for collision energy becomes less as the H_2 vibrational excitation increases. These results also show that vibrational excitation of the reactants is more efficient than translational energy in promoting the reaction. As shown in **Figure 6e** and **f**, the reaction thresholds in 4C process are higher than those of the CID ones. However, the reaction barrier of 4C process is lower than that of the CID process as shown in **Figure 1**. This can be attributed to the more severe dynamical constraints imposed on the former, such as the simultaneous requirement for two bond-breaking and two bond-forming processes.

In **Figure 6**, the ICSs are also compared with the previous full-dimensional quantum mechanical (QM) scattering results of Song et al.[65] on the BMKP PES. These authors have reported the ICSs for reactions between $H_2(v_1 = 10, 11, j_1 = 0)$ and $D_2(v_2 = 0, j_2 = 0)$. Since the QCT results on the two PESs are essentially the same as discussed, the QM results can be qualitatively compared with the QCT ones on the new PES, with the caveat that a D_2, rather than H_2 was used in the QM work. It is readily seen that the QM ICSs all follow the same trends as the QCT results: namely both the translational and vibrational excitations promote the reactions with the translational mode being more effective. However, the QM excitation functions have significantly lower thresholds than the QCT counterparts, clearly suggesting tunneling. The former is also quantitatively larger than the latter, although they are still on the same order of magnitude. This comparison underscores the importance of quantum effects

in these reactions.

The vibrational enhancement in these $H_2 + H_2$ reactive processes can be compared with another system that involves a 4C transition state. In a previous publication, the HH + H'OH' → HH' + HOH' system have been investigated and the reaction proceeds via a high energy 4C transition state, similar to the current system.[84] There, the CID asymptotes are significantly higher than the 4C barrier, so the later becomes dominant at energies below the CID threshold.

IV. Conclusions

In this work, we developed a new full-dimensional reactive PES for the H_4 system. Three reactive channels, namely CID, SE, 4C, are described by this global PES. The new PES is extended from the $H_2 + H_2$ nonreactive PES constructed by Zuo *et al.*,[42] which was fitted to 39,462 energy points at the level of MRCI/AV5Z using the high-fidelity PIP-NN method. To cover the three reactive channels, an additional 39,538 points were sampled and calculated at the same level of theory, amounting to a total of 79,000 points fitted by the same PIP-NN method. The final PES reproduces with high fidelity the properties of all the stationary points, as well as the MEPs of the SE and 4C channels. The fitting error of the new PIP-NN PES is only 0.6 meV, which is much lower than the previous BKMP PES (38.9 meV). This new PES thus provides a reliable platform for future dynamics studies of the reactions involving H_2 molecules.

This PES is expected to be more accurate than the BKMP PES in several aspects. First, the basis set used in the ab initio calculations is much larger. Second, there are more ab initio points used in the fitting of the PES. Finally, the use of the PIP-NN method significantly reduced the fitting error. This PES was used in preliminary dynamical calculations with a QCT method. Our results are in good agreement with those on the BKMP PES. Vibrational excitation of an H_2 reactant is found to enhance

the reactivity for all three reactive processes, which can be attributed to the strong coupling of the reactant vibrational modes with the reaction coordinate at each transition state. Finally, comparison with quantum scattering calculations suggests strong quantum effects.

The vibrational enhancement of the reactions studied here bodes well with the goal of vibrational control of reactivity, in which reactant vibrational excitation is needed to trigger the chemical transformation. Recent experimental advances, such as SARP[48] and SEP (stimulated emission pumping),[85] have demonstrated the ability to prepare single quantum states for molecules with significant vibrational excitation. Investigations of reactions involving such far-from-equilibrium species is an exciting opportunity within reach.

Notes

There are no conflicts of interest to declare.

The data that support the findings of this study are available from the corresponding author upon reasonable request.

Acknowledgments: This work is supported by a MURI grant from Army Office of Research (grant no. W911NF-19-1-0283 to NB and HG) and by the Spanish Ministry of Science and Innovation (grant nos. PID2021-122839NB-I00 to FJA and PID2020-113147GA-I00 to PGJ). JFEC gratefully acknowledges support from the Dodd-Walls Centre for Photonic and Quantum Technologies. The computation was performed at the Center for Advanced Research Computing (CARC) at UNM. HG thanks Prof. R. N. Zare for many stimulating discussions.

Supporting Information available: Fortran routines of the PES and test files.

References:

(1) Combes, F.; Pineau des Forêts, G. Molecular Hydrogen in Space. Cambridge University Press: Cambridge, 2000.

(2) Dove, J. E.; Rusk, A. C. M.; Cribb, P. H.; Martin, P. G. Excitation and dissociation of molecular hydrogen in shock waves at interstellar densities. *Astrophys. J.* **1987**, *318*, 379.

(3) Hodapp, K. W.; Davis, C. J. Molecular hydrogen outflows in W51. *Astrophys. J.* **2002**, *575*, 291.

(4) Stancil, P. C.; Lepp, S.; Dalgarno, A. The deuterium chemistry of the early universe. *Astrophys. J.* **1998**, *509*, 1-10.

(5) Galli, D.; Palla, F. The dawn of chemistry. *Annu. Rev. Astron. Astrophys.* **2013**, *51*, 163-206.

(6) Roueff, E.; Lique, F. Molecular excitation in the interstellar medium: Recent advances in collisional, radiative, and chemical processes. *Chem. Rev.* **2013**, *113*, 8906-8938.

(7) Neufeld, D. A.; Green, J. D.; Hollenbach, D. J.; Sonnentrucker, P.; Melnick, G. J.; Bergin, E. A.; Snell, R. L.; Forrest, W. J.; Watson, D. M.; Kaufman, M. J. Spitzer observations of hydrogen deuteride. *Astrophys. J.* **2006**, *647*, L33-L36.

(8) Schwenke, D. W. Calculations of rate constants for the three-body recombination of H_2 in the presence of H_2. *J. Chem. Phys.* **1988**, *89*, 2076-2091.

(9) Capitelli, M.; Cacciatore, M.; Celiberto, R.; De Pascale, O.; Diomede, P.; Esposito, F.; Gicquel, A.; Gorse, C.; Hassouni, K.; Laricchiuta, A.; et al. Vibrational kinetics, electron dynamics and elementary processes in H_2 and D_2 plasmas for negative ion production: modelling aspects. *Nucl. Fusion* **2006**, *46*, S260.

(10) de Graaf, M. J.; Severens, R.; Dahiya, R. P.; van de Sanden, M. C. M.; Schram, D. C. Anomalous fast recombination in hydrogen plasmas involving rovibrational excitation. *Phys. Rev. E* **1993**, *48*, 2098-2102.

(11) Krstić, P. S. Inelastic processes from vibrationally excited states in slow $H^+ + H_2$ and $H + H_2^+$ collisions: Excitations and charge transfer. *Phys. Rev. A* **2002**, *66*, 042717.

(12) Green, S. Rotational excitation in H_2-H_2 collisions: Close-coupling calculations. *J. Chem. Phys.* **1975**, *62*, 2271-2277.

(13) Schaefer, J. Rotational integral cross sections and rate coefficients of HD scattered by He and H_2. *Astron. Astrophys. Suppl. Ser.* **1990**, *85*, 1101-1125.

(14) Flower, D. R. The rotational excitation of H_2 by H_2. *Mon. Not. Royal Astron. Soc.* **1998**, *297*, 334-336.

(15) Flower, D. R. Vibrational relaxation of H_2 in collisions with rotationally excited H_2 molecules. *J. Phys. B: At. Mol. Opt. Phys.* **2000**, *33*, L193.

(16) Flower, D. R.; Roueff, E. Rovibrational relaxation in collisions between H_2 molecules: I. Transitions induced by ground state para-H_2. *J. Phys. B: At. Mol. Opt. Phys.* **1998**, *31*, 2935-2947.

(17) Flower, D. R.; Roueff, E. Rovibrational relaxation in collisions between H_2 molecules: II. Influence of the rotational state of the perturber. *J. Phys. B: At. Mol. Opt. Phys.* **1999**, *32*, 3399-3407.

(18) Pogrebnya, S. K.; Clary, D. C. A full-dimensional quantum dynamical study of vibrational relaxation in H_2+H_2. *Chem. Phys. Lett.* **2002**, *363*, 523-528.

(19) Lin, S. Y.; Guo, H. Full-dimensional quantum wave packet study of rotationally inelastic transitions in $H_2 + H_2$ collision. *J. Chem. Phys.* **2002**, *117*, 5183.

(20) Lin, S. Y.; Guo, H. Full-dimensional quantum wave packet study of collision-induced vibrational relaxation between para-H_2. *Chem. Phys.* **2003**, *289*, 191.

(21) Lin, S. Y.; Guo, H. Full-dimensional wave packet studies of vibrational relaxation of both para and ortho-H_2. *J. Phys. Chem. A* **2003**, *107*, 7197-7203.

(22) Gatti, F.; Otto, F.; Sukiasyan, S.; Meyer, H.-D. Rotational excitation cross sections of para-H2+para-H2 collisions. A full-dimensional wave-packet propagation study using an exact form of the kinetic energy. *J. Chem. Phys.* **2005**, *123*, 174311.

(23) Panda, A. N.; Otto, F.; Gatti, F.; Meyer, H.-D. Rovibrational energy transfer in ortho-H_2+para-H_2 collisions. *J.*

Chem. Phys. **2007**, *127*, 114310.
(24) Otto, F.; Gatti, F.; Meyer, H.-D. Rotational excitations in para-H_2+para-H_2 collisions: Full- and reduced-dimensional quantum wave packet studies comparing different potential energy surfaces. *J. Chem. Phys.* **2008**, *128*, 064305.
(25) Quéméner, G.; Balakrishnan, N. Quantum calculations of H_2–H_2 collisions: From ultracold to thermal energies. *J. Chem. Phys.* **2009**, *130*, 114303.
(26) Lee, T. G.; Balakrishnan, N.; Forrey, R. C.; Stancil, P. C.; Shaw, G.; Schultz, D. R.; Ferland, G. J. Rotational quenching rate coefficients for H_2 in collisions with H_2 from 2 to 10,000 K. *Astrophys. J.* **2008**, *689*, 1105-1111.
(27) Balakrishnan, N.; Quéméner, G.; Forrey, R. C.; Hinde, R. J.; Stancil, P. C. Full-dimensional quantum dynamics calculations of H_2–H_2 collisions. *J. Chem. Phys.* **2011**, *134*, 014301.
(28) Fonseca dos Santos, S.; Balakrishnan, N.; Lepp, S.; Quéméner, G.; Forrey, R. C.; Hinde, R. J.; Stancil, P. C. Quantum dynamics of rovibrational transitions in H_2-H_2 collisions: Internal energy and rotational angular momentum conservation effects. *J. Chem. Phys.* **2011**, *134*, 214303.
(29) Fonseca dos Santos, S.; Balakrishnan, N.; Forrey, R. C.; Stancil, P. C. Vibration-vibration and vibration-translation energy transfer in H_2-H_2 collisions: A critical test of experiment with full-dimensional quantum dynamics. *J. Chem. Phys.* **2013**, *138*, 104302.
(30) Balakrishnan, N.; Croft, J. F. E.; yang, B. H.; Forrey, R. C.; Stancil, P. C. Rotational quenching of HD in collisions with H_2: Resolving discrepancies for low-lying rotational transitions. *Astrophys. J.* **2018**, *866*, 95.
(31) Wan, Y.; Yang, B. H.; Stancil, P. C.; Balakrishnan, N.; Parekh, N. J.; Forrey, R. C. *Astrophys. J.* **2018**, *862*, 132.
(32) Wan, Y.; Balakrishnan, N.; Yang, B. H.; Forrey, R. C.; Stancil, P. C. Rotational quenching of HD induced by collisions with H_2 molecules. *Mon. Not. Royal Astron. Soc.* **2019**, *488*, 381-386.
(33) Croft, J. F. E.; Jambrina, P. G.; Aoiz, F. J.; Guo, H.; Balakrishnan, N. Cold collisions of ro-vibrationally excited D_2 molecules. *J. Phys. Chem. A* **2023**, *127*, 1619-1627.
(34) Zarur, G.; Rabitz, H. Effective potential formulation of molecule-molecule collisions with application to H_2–H_2. *J. Chem. Phys.* **1974**, *60*, 2057-2078.
(35) Boothroyd, A. I.; Dove, J. E.; Keogh, W. J.; Martin, P. G.; Peterson, M. R. Accurate ab initio potential energy computations for the H_4 system: Tests of some analytic potential energy surfaces. *J. Chem. Phys.* **1991**, *95*, 4331-4342.
(36) Aguado, A.; Suárez, C.; Paniagua, M. Accurate global fit of the H_4 potential energy surface. *J. Chem. Phys.* **1994**, *101*, 4004-4010.
(37) Diep, P.; Johnson, J. K. An accurate H_2–H_2 interaction potential from first principles. *J. Chem. Phys.* **2000**, *112*, 4465-4473.
(38) Boothroyd, A. I.; Martin, P. G.; Keogh, W. J.; Peterson, M. J. An accurate analytic H_4 potential energy surface. *J. Chem. Phys.* **2002**, *116*, 666-689.
(39) Hinde, R. J. A six-dimensional H_2–H_2 potential energy surface for bound state spectroscopy. *J. Chem. Phys.* **2008**, *128*, 154308.
(40) Patkowski, K.; Cencek, W.; Jankowski, P.; Szalewicz, K.; Mehl, J. B.; Garberoglio, G.; Harvey, A. H. Potential energy surface for interactions between two hydrogen molecules. *J. Chem. Phys.* **2008**, *129*, 094304.
(41) Garberoglio, G.; Jankowski, P.; Szalewicz, K.; Harvey, A. H. Second virial coefficients of H_2 and its isotopologues from a six-dimensional potential. *J. Chem. Phys.* **2012**, *137*, 154308.
(42) Zuo, J.; Croft, J. F. E.; Yao, Q.; Balakrishnan, N.; Guo, H. Full-dimensional potential energy surface for ro-vibrationally inelastic scattering between H_2 molecules. *J. Chem. Theo. Comput.* **2021**, *17*, 6747-6756.
(43) Perreault, W. E.; Mukherjee, N.; Zare, R. N. Quantum control of molecular collisions at 1 kelvin. *Science* **2017**, *358*, 356-359.
(44) Perreault, W. E.; Mukherjee, N.; Zare, R. N. Cold quantum-controlled rotationally inelastic scattering of HD

with H_2 and D_2 reveals collisional partner reorientation. *Nat. Chem.* **2018**, *10*, 561-567.
(45) Zhou, H.; Perreault, W. E.; Mukherjee, N.; Zare, R. N. Shape resonance determined from angular distribution in D_2 (v = 2, j = 2) + He $\rightarrow$ D_2 (v = 2, j = 0) + He cold scattering. *J. Chem. Phys.* **2021**, *154*, 104309.
(46) Zhou, H.; Perreault, W. E.; Mukherjee, N.; Zare, R. N. Quantum mechanical double slit for molecular scattering. *Science* **2021**, *374*, 960-964.
(47) Zhou, H.; Perreault, W. E.; Mukherjee, N.; Zare, R. N. Anisotropic dynamics of resonant scattering between a pair of cold aligned diatoms. *Nat. Chem.* **2022**, *14*, 658-663.
(48) Mukherjee, N. Quantum-controlled collisions of H_2 molecules. *J. Phys. Chem. A* **2023**, *127*, 418-438.
(49) Croft, J. F. E.; Balakrishnan, N.; Huang, M.; Guo, H. Unraveling the stereodynamics of cold controlled HD-H_2 collisions. *Phys. Rev. Lett.* **2018**, *121*, 113401.
(50) Jambrina, P. G.; Croft, J. F. E.; Guo, H.; Brouard, M.; Balakrishnan, N.; Aoiz, F. J. Stereodynamical control of a quantum scattering resonance in cold molecular collisions. *Phys. Rev. Lett.* **2019**, *123*, 043401.
(51) Jambrina, P. G.; Croft, J. F. E.; Zuo, J.; Guo, H.; Balakrishnan, N.; Aoiz, F. J. Stereodynamical control of cold collisions between two aligned D_2 molecules. *Phys. Rev. Lett.* **2023**, *130*, 033002.
(52) Balakrishnan, N.; Jambrina, P. G.; Croft, J. F. E.; Guo, H.; Aoiz, F. J. Quantum stereodynamics of cold molecular collisions. *Chem. Commun.* **2024**, *in press (DOI: 10.1039/D3CC04762H)*.
(53) Bauer, S. H. Four center metathesis reactions. *Annu. Rev. Phys. Chem.* **1979**, *30*, 271-310.
(54) Hernandez, M. I.; Clary, D. C. Four-center reactions: A quantal model for H4. *J. Chem. Phys.* **1996**, *104*, 8413-8423.
(55) Martin, P. G.; Keogh, W. J.; Mandy, M. E. Collision-induced dissociation of molecular hydrogen at low densities. *Astrophys. J.* **1998**, *499*, 793.
(56) Ceballos, A.; Garcia, E.; Rodriguez, A.; Laganà, A. Quasiclassical kinetics of the H_2 + H_2 reaction and dissociation. *J. Phys. Chem. A* **2001**, *105*, 1797-1804.
(57) di Domenico, D.; Hernández, M. I.; Campos Martínez, J. Wave packet calculations for $H_2(v_1=10–14)+H_2(v_2=0–2)$: Reaction and dissociation mechanisms. *J. Chem. Phys.* **2001**, *115*, 7897-7906.
(58) Hernández, M. I.; Campos-Martínez, J.; Van Caillie, C.; Di Domenico, D. Wave packet calculations for H_2+H_2 collisions: isotopic substitution effects. *Mole. Phys.* **2004**, *102*, 2335-2343.
(59) Lu, Y.; Zhang, D. H.; Lee, S.-Y. A time-dependent wave packet study of the H_4 four-center reaction. *Chem. Phys.* **2005**, *308*, 217-224.
(60) Garcia, E.; Saracibar, A.; Sánchez, C.; Laganà, A. Effect of the total angular momentum on the dynamics of the H_2 + H_2 system. *J. Phys. Chem. A* **2009**, *113*, 14312-14320.
(61) Lu, Y.; Lee, S.-Y.; Zhang, D. H. A full dimensional time-dependent wave packet study for the H4 four-center, collision induced dissociation, and single exchange reactions: Reaction probabilities for J=0. *J. Chem. Phys.* **2006**, *124*, 011101.
(62) Carmona-Novillo, E.; Bartolomei, M.; Hernández, M. I.; Campos-Martínez, J. Quasiclassical trajectory study of reactive and dissociative processes in H_2+H_2: Comparison with quantum-mechanical calculations. *J. Chem. Phys.* **2007**, *126*.
(63) Song, H.; Lu, Y.; Lee, S.-Y. Three-dimensional wave packet dynamics of H_2+D_2 reaction. *Chem. Phys.* **2011**, *381*, 72-79.
(64) Song, H.; Lu, Y.; Lee, S.-Y. Full-dimensional time-dependent wave packet dynamics of H_2 + D_2 reaction. *J. Chem. Phys.* **2011**, *135*, 014305.
(65) Song, H.; Lu, Y.; Lee, S.-Y. Fully converged integral cross sections of collision induced dissociation, four-center, and single exchange reactions, and accuracy of the centrifugal sudden approximation in H_2 + D_2 reaction. *J. Chem. Phys.* **2012**, *136*, 114307.
(66) Hoffmann, R. Transition state for the hydrogen–iodine and the hydrogen exchange reactions. *J. Chem. Phys.*

2003, *49*, 3739-3740.
(67) Lee, T.-G.; Balakrishnan, N.; Forrey, R. C.; Stancil, P. C.; Schultz, D. R.; Ferland, G. J. State-to-state rotational transitions in H_2+H_2 collisions at low temperatures. *J. Chem. Phys.* **2006**, *125*, 114302.
(68) Knowles, P. J.; Werner, H.-J. An efficient method for the evaluation of coupling coefficients in configuration interaction calculations. *Chem. Phys. Lett.* **1988**, *145*, 514-522.
(69) Werner, H.-J.; Follmeg, B.; Alexander, M. H. Adiabatic and diabatic potential energy surfaces for collisions of CN($X\,^2\Sigma^+$, $A\,^2\Pi$) with He. *J. Chem. Phys.* **1988**, *89*, 3139-3151.
(70) Dunning, T. H. Gaussian basis sets for use in correlated molecular calculations. I. The atoms boron through neon and hydrogen. *J. Chem. Phys.* **1989**, *90*, 1007-1023.
(71) Kendall, R. A.; Dunning, T. H.; Harrison, R. J. Electron affinities of the first-row atoms revisited. Systematic basis sets and wave functions. *J. Chem. Phys.* **1992**, *96*, 6796-6806.
(72) Jiang, B.; Guo, H. Permutation invariant polynomial neural network approach to fitting potential energy surfaces. *J. Chem. Phys.* **2013**, *139*, 054112.
(73) Li, J.; Jiang, B.; Guo, H. Permutation invariant polynomial neural network approach to fitting potential energy surfaces. II. Four-atom systems. *J. Chem. Phys.* **2013**, *139*, 204103.
(74) Werner, H. J.; Knowles, P. J.; Knizia, G.; Manby, F. R.; Schütz, M. Molpro: a general-purpose quantum chemistry program package. *WIREs Comput. Mol. Sci.* **2012**, *2*, 242-253.
(75) Langhoff, S. R.; Davidson, E. R. Configuration interaction calculations on nitrogen molecule. *Int. J. Quant. Chem.* **1974**, *8*, 61-72.
(76) Braams, B. J.; Bowman, J. M. Permutationally invariant potential energy surfaces in high dimensionality. *Int. Rev. Phys. Chem.* **2009**, *28*, 577–606.
(77) Xie, Z.; Bowman, J. M. Permutationally invariant polynomial basis for molecular energy surface fitting via monomial symmetrization. *J. Chem. Theo. Comput.* **2010**, *6*, 26–34.
(78) Raff, L. M.; Komanduri, R.; Hagan, M.; Bukkapatnam, S. T. S. *Neural Networks in Chemical Reaction Dynamics*; Oxford University Press, Oxford, 2012.
(79) Hase, W. L.; Duchovic, R. J.; Hu, X.; Komornicki, A.; Lim, K. F.; Lu, D.-H.; Peslherbe, G. H.; Swamy, K. N.; Linde, S. R. V.; Varandas, A.; et al. VENUS96: A General Chemical Dynamics Computer Program. *Quantum Chemistry Program Exchange Bulletin* **1996**, *16*, 671.
(80) Gutzwiller, M. C. *Chaos in Classical and Quantum Mechanics*; Springer, New York, 1990.
(81) Jiang, B.; Li, J.; Guo, H. Potential energy surfaces from high fidelity fitting of ab initio points: The permutation invariant polynomial-neural network approach. *Int. Rev. Phys. Chem.* **2016**, *35*, 479-506.
(82) Polanyi, J. C. Concepts in reaction dynamics. *Acc. Chem. Res.* **1972**, *5*, 161-168.
(83) Guo, H.; Jiang, B. The sudden vector projection model for reactivity: Mode specificity and bond selectivity made simple. *Acc. Chem. Res.* **2014**, *47*, 3679-3685.
(84) Li, J.; Liu, Y.; Guo, H.; Li, J. An accurate full-dimensional H_4O potential energy surface and dynamics of an exchange reaction. *Phys. Chem. Chem. Phys.* **2022**, *24*, 27548-27557.
(85) Perera, C. A.; Amarasinghe, C.; Guo, H.; Suits, A. G. Cold collisions of hot molecules. *Phys. Chem. Chem. Phys.* **2023**, *25*, 22595-22606.

Table 1. Energies (eV) and vibrational harmonic frequencies (cm^{-1}) of the stationary points for the $H_2 + H_2$ system.

Species	Method	*E*	Frequencies						
			1	2	3	4	5	6	7
H_2+H_2	PIP-NN PES [a]	0	4405		4405				
	MRCI/AV5Z [b]	0	4400		4400				
	BMKP PES [c]	0	4404		4404				
TS1	PIP-NN PES [a]	4.827	*i*517	141	141	406	406	551	3968
	MRCI/AV5Z [b]	4.827	*i*528	144	144	410	410	559	3952
	BMKP PES [c]	4.830	*i*586	69	69	430	430	539	3958
TS2	PIP-NN PES [a]	4.532	*i*3158	1229	1350	1523	1654	3701	
	MRCI/AV5Z [b]	4.532	*i*3163	1227	1348	1513	1656	3706	
	BMKP PES [c]	4.505	*i*2776	1247	1437	1768	2116	4063	
$H+H_2+H$	PIP-NN PES [a]	4.746	4405						
	MRCI/AV5Z [b]	4.746	4400						
	BMKP PES [c]	4.746	4404						

[a]: This work, PIP-NN PES; [b]: This work, MRCI/AV5Z. [c]: The BMKP PES at MRD-CI/ (9s3p1d)/[4s3p1d] level.[38]

Table 2. Results of the SVP model for the TS1 and TS2 on the PIP-NN PES.

	TS1	TS2
v_{H_2}	0.536	0.507
H_2 rotation	0.000	0.001
Translation	0.665	0.659

Figure 1. Schematic reaction paths for the $H_2 + H_2$ system. The geometric and energetic values of the stationary points from the PIP-NN PES, MRCI/AV5Z, and BMKP PES are shown from top to bottom. Energies are in eV and relative to the $H_2 + H_2$ asymptote. All distances are in Å.

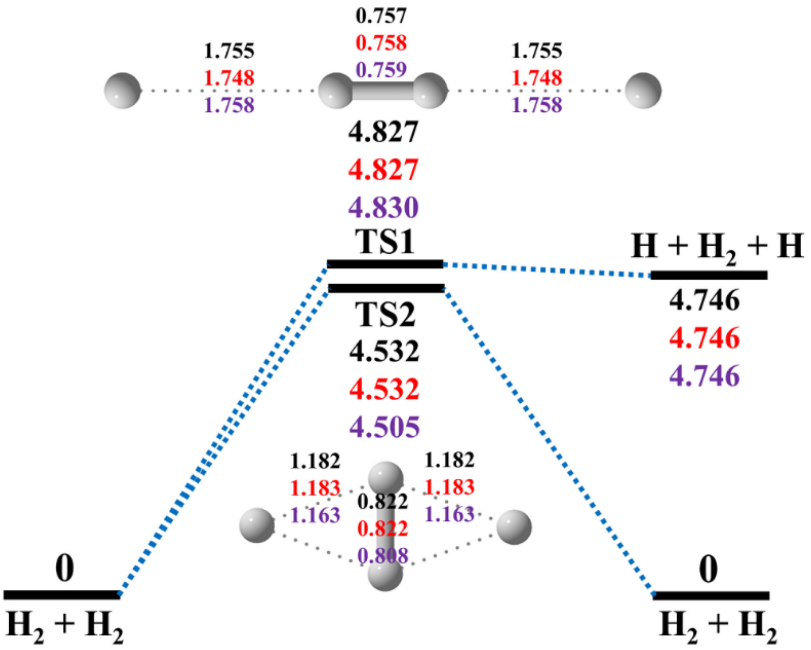

Figure 2. (a) Fitting error (E_{fit} - E_{target}, in eV) of the PIP-NN PES as a function of the ab initio energy (eV). (b) Distribution of the absolute fitting errors. The bin size is 0.1 meV.

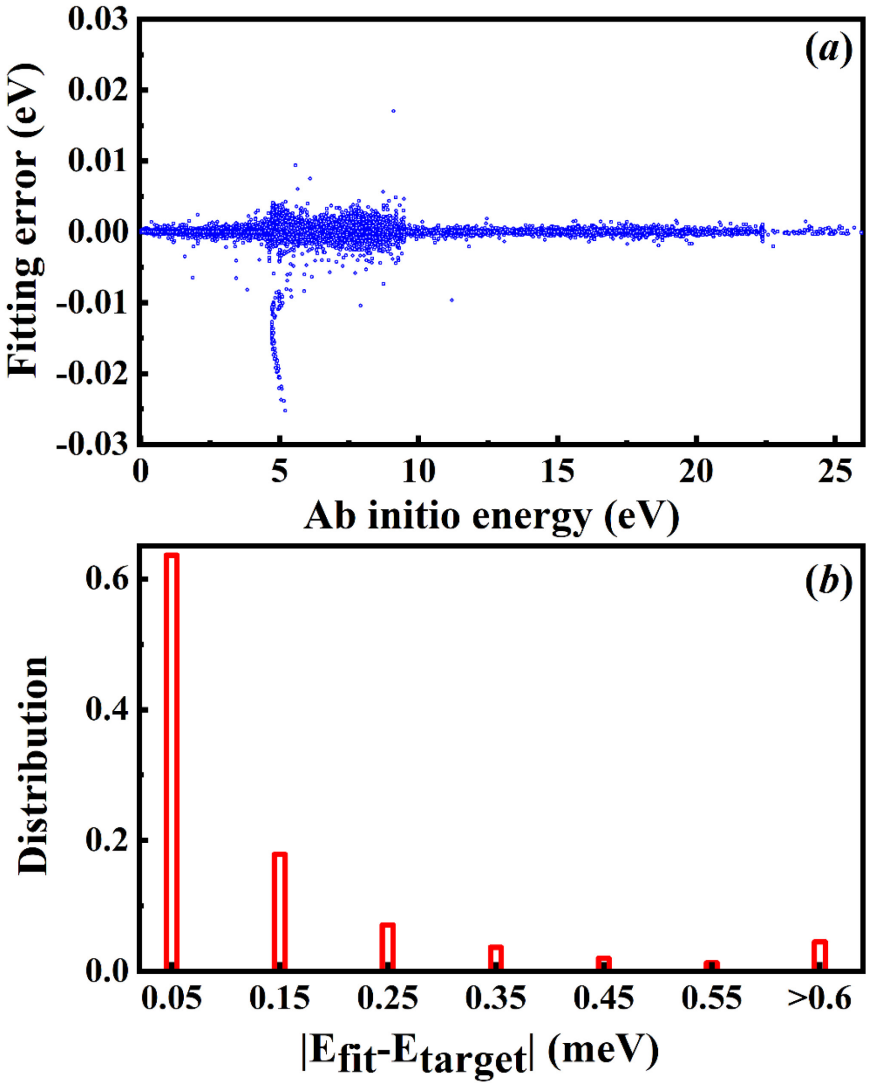

Figure 3. Potential energies along MEPs of TS1 and TS2 on the PIP-NN PES. The symbols represent the *ab initio* calculated energies. The geometries of the stationary points are shown.

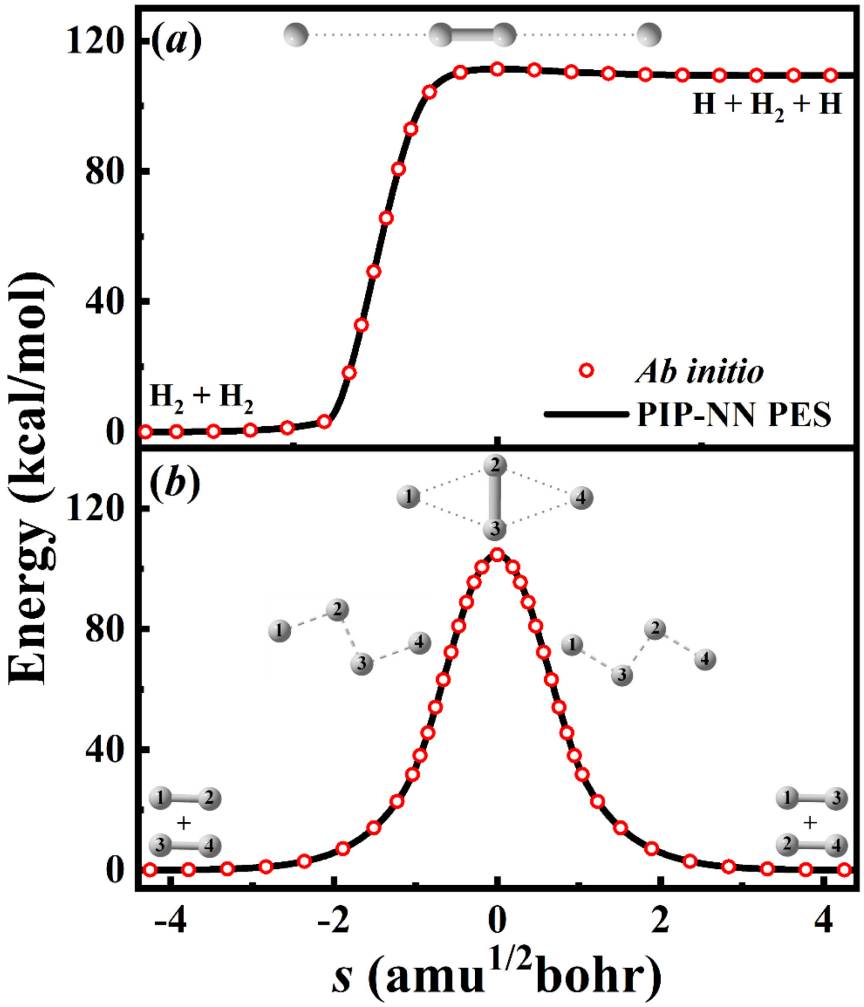

Figure 4. Contours of the PES (eV) for the reactive dissociation channel as a function of R_1 and R_2. All other coordinates are fixed at TS1. The definition of R_1 and R_2 is shown in the inset.

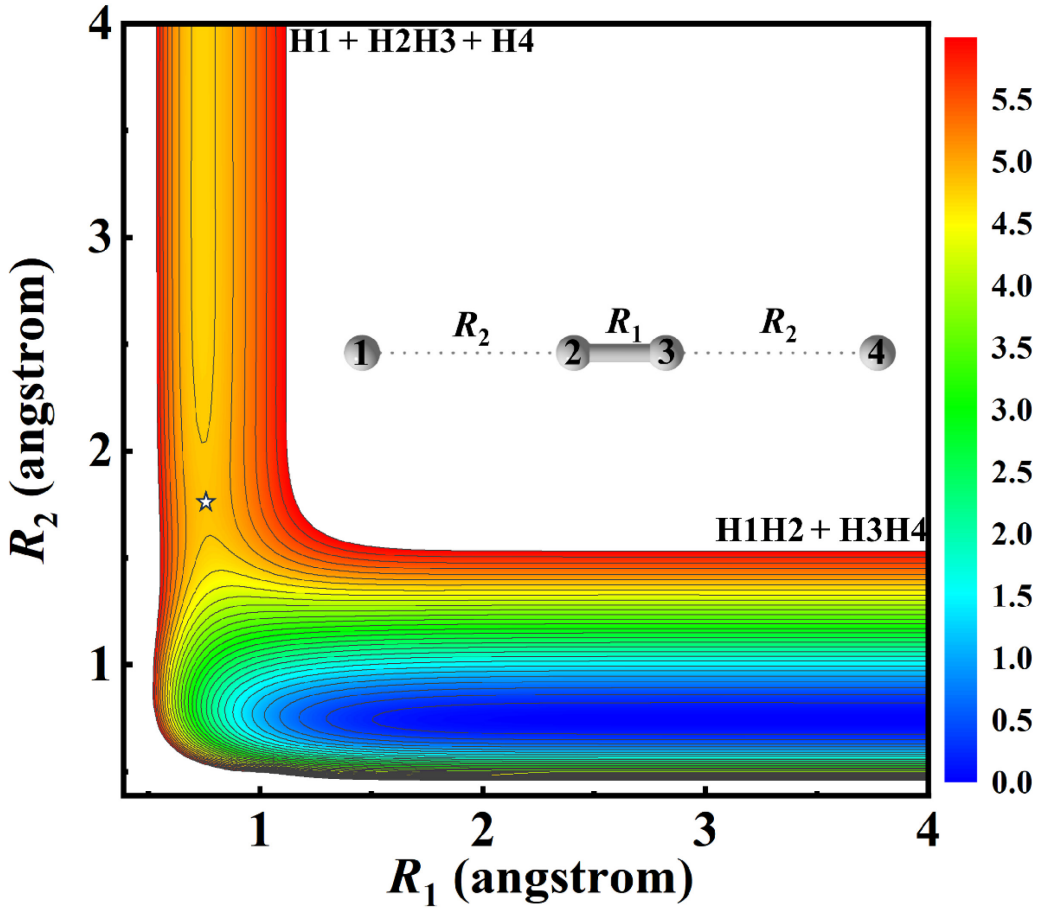

Figure 5. Contours of the PES (eV) for the 4C channel as a function of R_1 and R_2 with other coordinates fixed at TS2. The definition of R_1 and R_2 is shown in the inset.

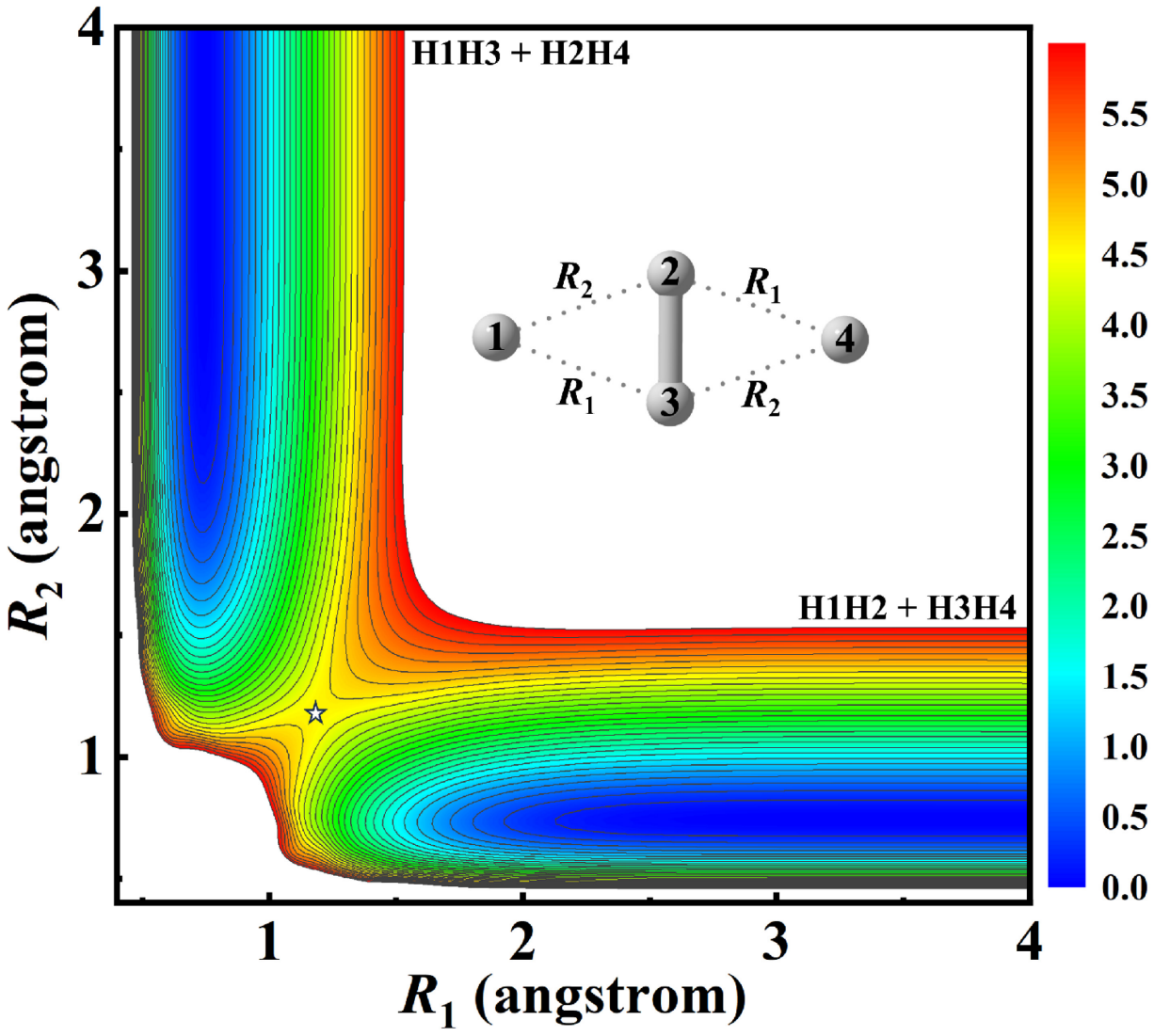

Figure 6. ZPE-corrected QCT integral cross sections (ICSs) of the CID (upper panels), 4C (central panels), and SE (lower panels) channels for H_2 (v_1 = 10, 11, 12, 13, j_1 = 0) + H_2 (v_2 = 0, j_2 = 0) as a function of the collision energy (left-hand panels) and total energy (right-hand panels). Solid lines represent results on the PIP-NN PES, dotted lines refer to the BMKP PES ones and dashed lines are the QM results.

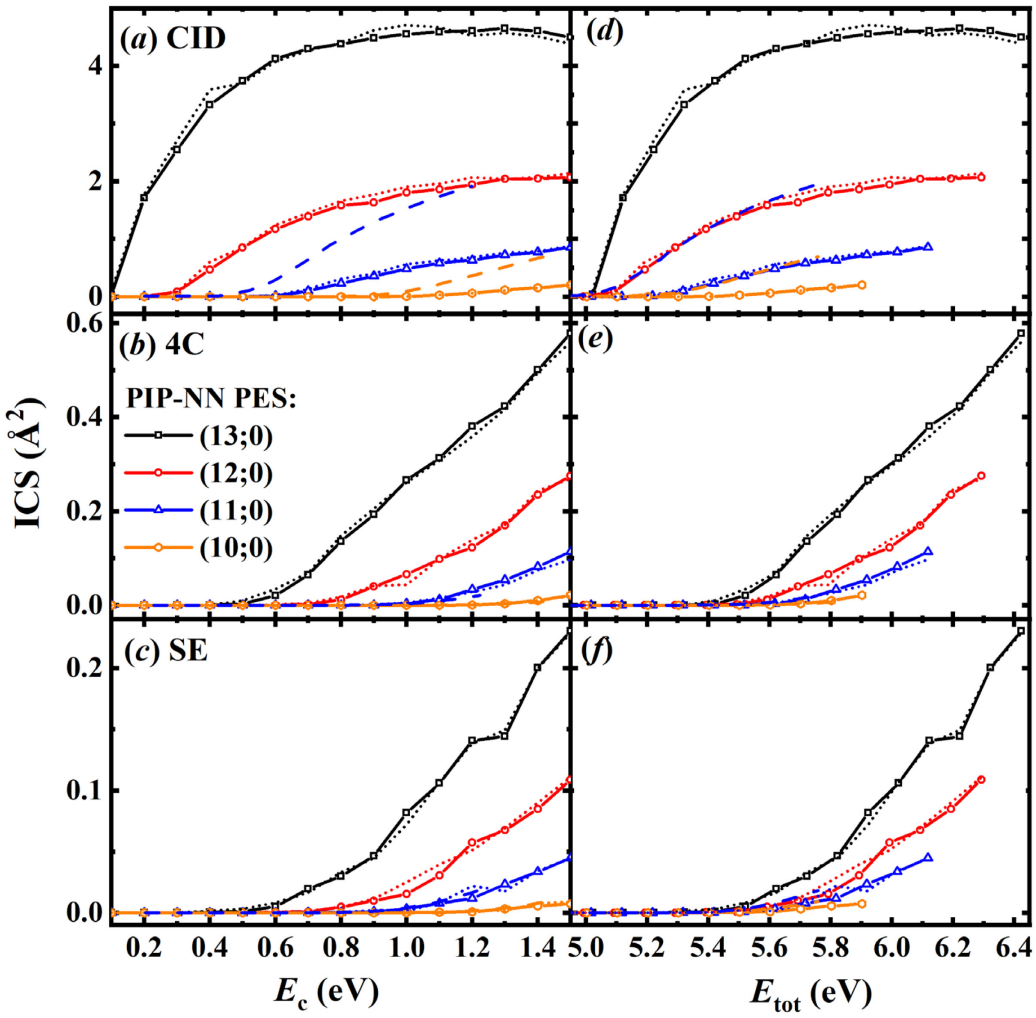

TOC graphic